Liquid Phase Separation in Cu-Co-Fe and Cu-Fe-Ni-Cr Alloys

A. Munitz, R. Abbachian*, C. Cotler and C. Shacham

Nuclear Research Center, Negev, P.O. Box 9001, Israel
**Chairman, Department of Material Science and Engineering, University of Gainesville, Florida, USA*

ABSTRACT

The impact of cooling rate on the microstructure of Cu-Co-Fe and Cu-Fe-Ni-Cr alloys was investigated by using scanning electron microscopy. The relatively high cooling rates during arc melting and electron beam surface melting of the alloys result in bulk supercooling, which in turn causes three microstructural effects: 1) Melt separation into two liquids, copper poor-L1 and copper rich-L2, 2) microstructural refinement, and 3) enhanced solute trapping of Cu in the α-Fe phase.

1. INTRODUCTION

The bonding between stainless steel and copper has many industrial applications, such as in heat exchangers and safes, where the unique properties of the two materials are required, e.g., the heat conductivity of copper and corrosion resistance of the stainless steel. The bonding may be achieved by explosive bonding of two plates or by welding [Tungsten Inert Gas (TIG) or electron beam (EB) welding] /1,2/. In previous studies we have found /2,3/ that solidification of Fe-Cu alloys at high cooling rates, such as resolidification of electron beam melted surfaces /3/, and molten pockets in explosively bonded Fe-Cu plates /1/, induces dynamic bulk melt supercooling. It was found that when Cu-Fe alloys are supercooled below a certain temperature, T_{SEP}, which depends on its composition, the liquid metal enters into a metastable liquid miscibility gap, and separates into two liquids: an iron-rich melt (L1), and a copper-rich melt (L2). Each melt then solidifies on a path dictated by the stable phase diagram boundary. It was also found that TIG and electron beam welding between stainless steel and copper tubes causes melt separation into two liquids /2/.

The present work was aimed towards better understanding of the phenomenon of liquid melt separation in Cu-Fe-Co and Cu-Fe-Ni-Cr systems. Also there is meager information on the stable phase diagrams of these systems.

2. EXPERIMENTAL

High purity copper (99.98%), high purity iron (99.99%) and high purity cobalt (99.99%) were used to prepare ten Cu-Fe-Co alloys containing various compositions. Concurrently, commercial Cu and commercial stainless steel were used to prepare four specimens with different compositions. The specimens with the desired compositions were arc melted with a non-consumable tungsten electrode followed by electron beam surface melting. It was necessary to obtain a higher degree of surface mixing for samples used for the electron beam surface melting. Consequently, for these samples several remelting cycles were performed, with the specimen turned upside down before each remelting. The surface of the processed samples were flattened by abrading one side with Sic papers up to 600#. Then the surfaces were melted with an electron beam having a driving voltage of 60 kV, a current between 4 and 10 mA, and a scanning velocity of about 5 m/min. The electron beam was focused about 1 mm beneath the molten surface. The cooling rates achieved using this technique are estimated to be as high as 10^6 K/sec /4,5/. After solidification, the samples were cross-sectioned and prepared using standard

metallographic procedures. The specimens were etched in a solution which comprised 120 ml H_2O, 10 g ammonium cupric chloride and enough ammonium hydroxide to dissolve all of the ammonium cupric chloride crystals. The etching time ranged between 5 and 12 seconds. The microstructures and compositional profiles were investigated using a scanning electron microscope with energy dispersive spectroscopy (EDS) capabilities. For the energy dispersive spectroscopy analysis, the specimens were etched very lightly in order to reveal the microstructure yet keep the surface roughness to a minimum. The raw intensity data were corrected with a standard ZAF computer program /6/.

3. RESULTS AND DISCUSSION

3.1 Solidification of Cu-Fe-Co alloys at different cooling rates

Secondary electron images (SEMs) illustrating the microstructure of Cu-Fe-Co specimens are illustrated in Figures 1 and 2. Secondary electron images illustrating the microstructure of Cu-24.0 wt.% Fe-19.2 wt.% Co are presented in Figure 1. In Figure 1a, a general view of the penetration of the fused zone into the substrate is shown. The substrate, which can be seen at the bottom of the micrograph and in greater magnification in Figure 1b, consisted of primary Fe and Co-rich dendrites embedded in a Cu-rich matrix. The fusion line between the fused zone and the matrix is shown in Figure 1c. Unmelted primary dendrites are seen to protrude into the fused zone. It is reasonable to assume that only the Cu-rich matrix has been melted and solidified epitaxially on the Cu-rich solid in the matrix. However, about 15 μm above the fusion line there is a morphology transition from a plane front solidification to a microstructure characteristic of solidification in the miscibility gap. In this case the microstructure consisted of spherical particles which uniformly covered the area embedded in a copper matrix, as shown in Figures 1d to 1f. The structure consists of tiny spheres embedded in a matrix. The appearance of spherulites of one composition in a matrix of another composition implies that liquid phase separation occurred prior to solidification /3,8/. As was found in previous work /3,8,9/, bulk supercooling of alloys which undergo liquid phase separation below a certain temperature (T_{SEP}) resulted in the separation of the melt into two liquids: one poor in Cu called L1, and a second liquid rich in Cu called L2. Each melt then solidifies on a path dictated by the stable phase diagram boundary. Usually, one liquid solidifies as spheres and the other as the matrix. Due to the short solidification time and the large convection involved in the process of EB surface melting, the spheres have a small diameter.

The solidification of electron beam surface melted specimens is complex. At the fusion line, the thermal gradient, G, is very large. The interface velocity, R, is very small, thus G/R is very large. According to the classical constitutional supercooling criterion /10/, the conditions for plane front solidification thus exist, and a plane front growth takes place. As solidification proceeds, the thermal gradients decrease, and the interface velocities increase. Thus, G/R decreases markedly. As the solidified front reaches about 15 μm from the fusion line, the value G/R decreases to a value thermodynamically favorable for melt separation to take place. As proposed in some of our previous publications /3,8/, considerable dynamic supercooling could take place up to a level of 150 K due to the larger heat transport compared to the mass transport. Such high supercooling levels might cause melt separation (i.e., Co-rich spheres embedded in a Cu-rich melt).

The microstructure of Cu 12.1 wt.% Fe-11.3 wt.% Co is illustrated in Figure 2. The microstructure of the arc-melted specimen consisted of two regions: i) Up to 200 μm from the Cu chill (region I in Figure 2b) the microstructure consisted of three types of structures: spherical particles with dendrites attached to them (Figure 2c), Fe-Co-rich dendrites embedded in a Cu-rich matrix, and ii) The rest of the sample (region II in Figure 2b) contained primary Fe+Co rich dendrites embedded in a Cu-rich matrix. As reported in a previous work /8/, and as calculated by Clyne /11/, due to the large heat absorption near the Cu chill, melt bulk supercooling might be obtained up to regions of 200 μm. This supercooling might cause melt separation in certain melt compositions as was actually observed. The microstructure in the fused zone consisted of spheres embedded in a Cu-rich matrix. The spheres near the fusion line are smaller (Figure 2e) than the

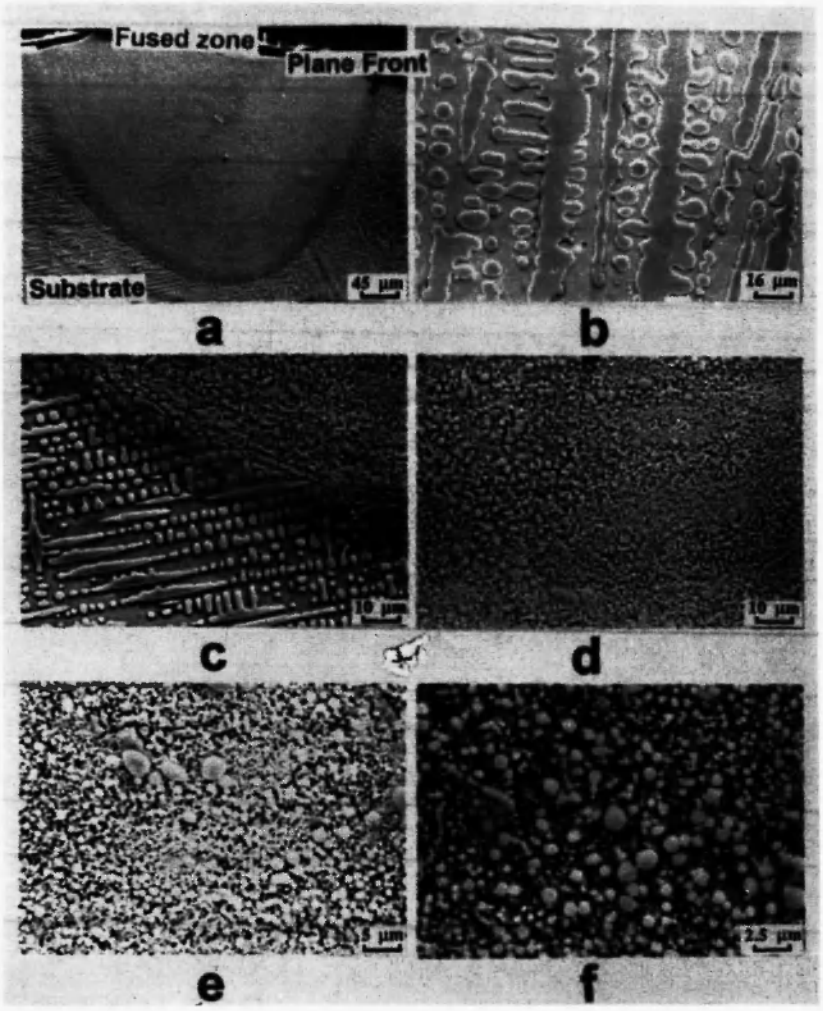

Fig. 1: Secondary electron images illustrating an electron beam melted surface of an arc-melted Cu-24.0 wt.% Fe-19.2 wt.% Co alloy, (a) an overall view, (b) arc melt microstructure, (c) higher magnification of EB fused path and its vicinity, (d)-(f) different magnifications of the fused zone.

spheres far from the fusion line (Figure 2f). However, both spheres are at least one order of magnitude smaller than the spheres observed in the arc-melted samples. The differences in the sizes were caused by the difference in solidification time. The shorter the solidification time (near the fusion line), the smaller the spherical particles.

3.2. Microstructure of Cu-Fe-Ni-Cr Alloys

Secondary electron images illustrating the microstructure of Cu-Fe-Ni-Cr alloys are presented in Figures 3 and 4. The microstructure of arc melt as well as EB melted surfaces of Cu-15.9 wt.% Fe-2.3 wt.% Ni-4.7 wt.% Cr are illustrated in Figure 3. The microstructure of the arc-melted surface consisted of three different phases: spherical particles with dendrite structure growing attached to them (Figures 3b and 3c), Fe-Ni-Cr-rich dendrites embedded in a Cu-rich matrix. The composition of the different phases is summarized in Table 1. The microstructure of the fused zone is given in Figures 3d through 3f. As described earlier, up to 15 μm from the fusion line a plane front solidification takes place (Figure 3d). Original spheres that did not have sufficient time to dissolve due to the short dwell time duration in the melt could be observed up to 30 mm from the fusion line. Further away from the fusion

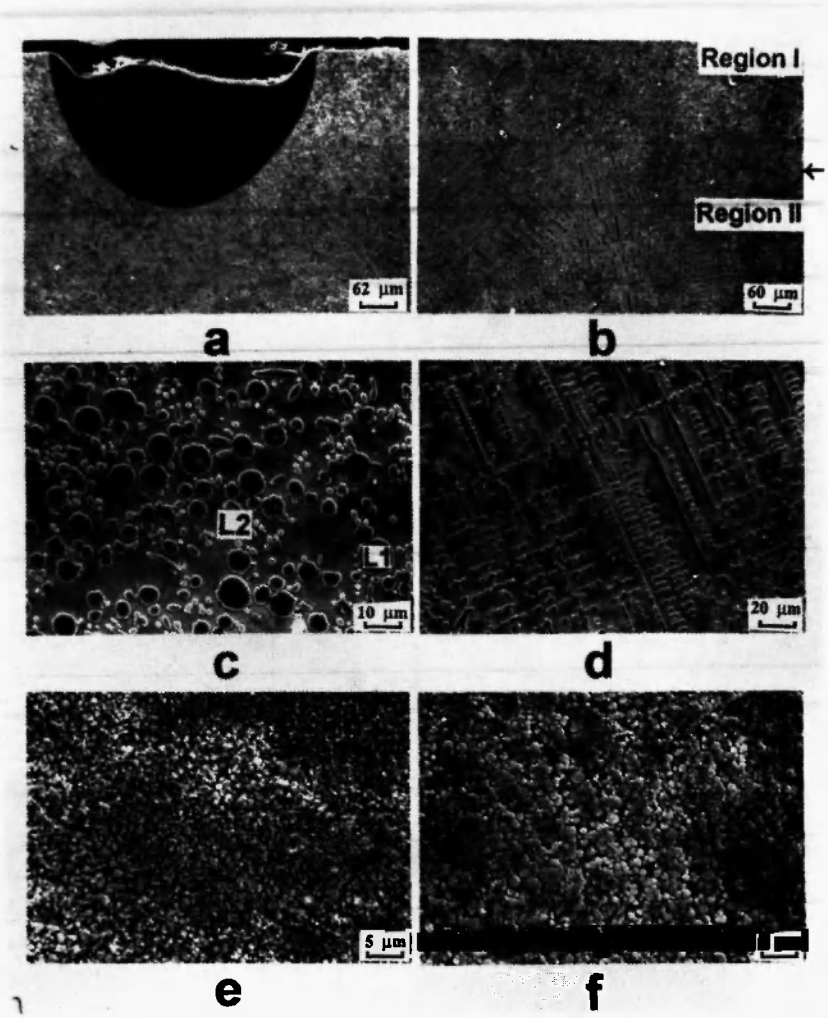

Fig. 2: Secondary electron images illustrating an electron beam melted surface of an arc-melted Cu-12.1 wt.% Fe-11.3 wt.% Co alloy. (a) an overall view, (b) arc melt microstructure at low magnification, (c) higher magnification arc melt microstructure demonstrating melt separation, (d) dendritic arc-melt microstructure, (e) higher magnification of the fused zone near the fusion line, (f) higher magnification of the fused zone far from the fusion line.

line the microstructure of the fused zone changed gradually to a structure characteristic of melt separation under high cooling rates (Figures 3e and 3f).

The microstructure of Cu-47.3 wt.% Fe-5.1 wt.% Ni-14.1 wt.% Cr is presented in Figure 4. The macro-structure consisted of two colors (Figure 4a): (i) Bright phase which was identified as primary L2 (Cu-rich) liquid, and (ii) Dark phase identified as the primary L1 (Fe-Ni-Cr-rich) liquid. The composition of the various phases is shown in Table 2. As can be seen from Figure 4a, massive melt separation has occurred (almost complete melt separation). Such massive separation was observed in all samples which contained less than 50 wt.% Cu. This massive melt separation might result from there being C in the alloys. Because of the massive melt separation, the original melt became uneven. In the extreme case, like in our case, two regions of different composition were created during the arc melting. This influences the EB fused zone. Indeed, as we shall see later, two types of fused zone were observed, each one belonging to a different melt, which has different characteristics.

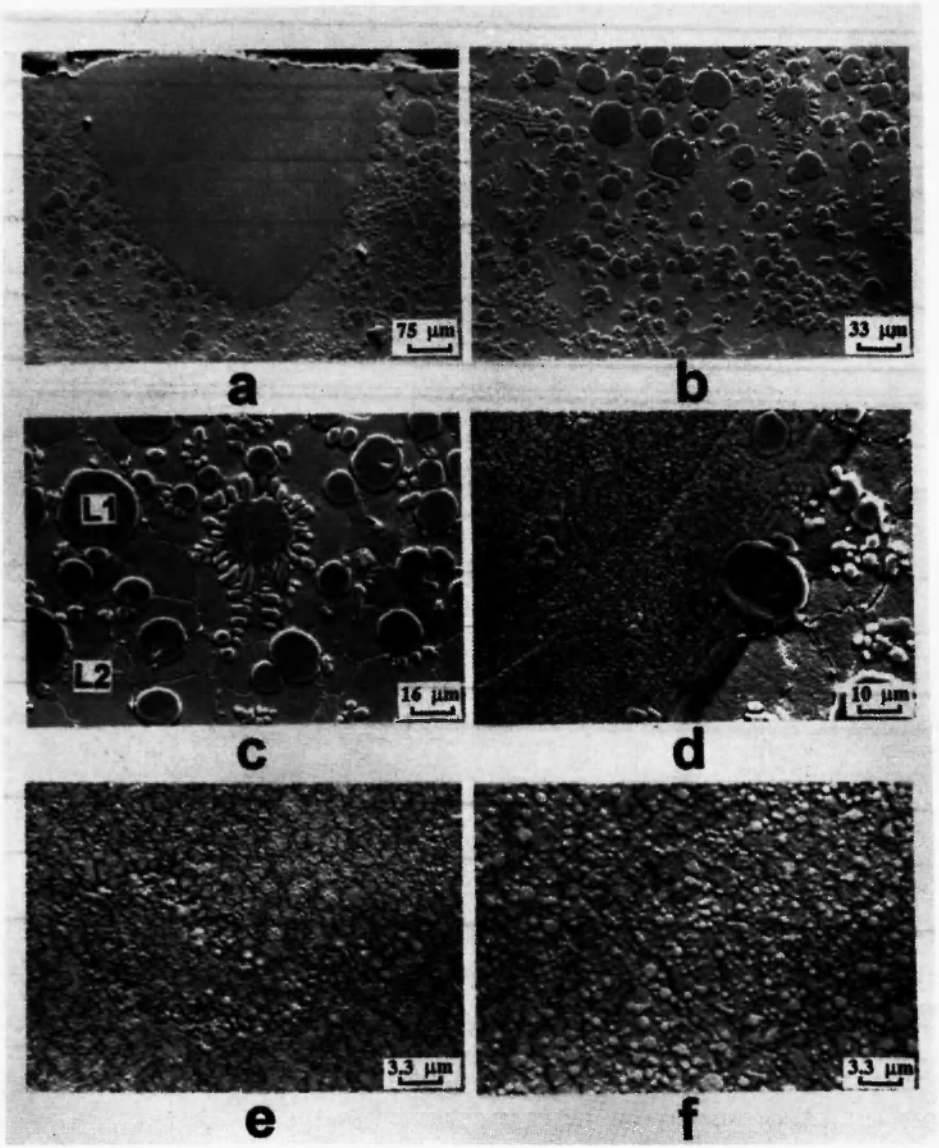

Fig. 3: Secondary electron images illustrating an electron beam melted surface of an arc melted Cu-15.9 wt.% Fe-2.3 wt.% Ni-4.7 wt.% Cr alloy. (a) an overall view of EB fused path and its vicinity, (b)-(c) arc melt microstructure in two magnifications, (d) higher magnification of the fusion line, (d)-(f) different magnification of the fused zone.

Table 1

The composition of the different phases for Cu-15.9 wt.% Fe-2.3 wt.% Ni-4.7 wt.% Cr

Phase description	Cu wt.%	Fe wt.%	Ni wt.%	Cr wt.%
Average composition	77.1	15.9	2.3	4.7
Spheres (L1)	19.3	58.7	6.7	15.4
Matrix (L2)	69.7	20.5	4.0	6.2
smooth part in matrix	95.8	0.8	2.3	1.1
Dendrites	16.6	61.4	7.4	14.3
Average EB fused zone	74.5	18.5	2.4	4.6

Table 2
The composition of the different phases for Cu-47.3 wt.% Fe-5.1 wt.% Ni-14.1 wt.% Cr.

Phase description		Cu wt.%	Fe wt.%	Ni wt.%	Cr wt.%
Average composition		33.5	47.3	5.1	14.17
Primary L1	Average composition	28.4	15.6	5.1	15.5
	Secondary L2 spheres	76.4	15.6	3.3	15.7
	Dendrites in L2 spheres	90.5	5.0	3.1	1.4
	Grains in L2 sphere	13.0	64.5	6.3	16.2
	Secondary L1 matrix	5.2	66.7	4.1	24.0
	L1 second phase	87.5	7.6	3.1	1.8
Primary L2	Average composition	61.9	26.1	4.5	7.5
	Secondary L2 matrix	67.7	21.9	4.2	6.2
	Secondary L1 spheres	17.6	58.9	6.9	16.6
	Average EB	69.6	21.0	3.9	5.5
	L1 sphere in EB	37.5	44.6	6.2	11.7

In Figures 4b and 4c we present the microstructure of the primary L1 zone. As can be seen from Figure 4b, the microstructure is composed of spheres in a matrix with L2 composition. This indicates that secondary phase separation has taken place. This secondary phase separation in the arc-melt specimens was observed only for specimens with less than 50 wt.% Cu. EB surface melting of such a composition caused massive cracking in the fused zone (Figure 4b. No melt separation was observed in the fused zone, as can be seen from Figure 4d. The microstructure of the primary L2 phase is shown in Figure 4e. The dark phase is a secondary L1 separation. The EB fused zone shows clear evidence of secondary melt separation (Figure 4f).

The actual amount of each liquid and their shape in the solidified samples depend on four major factors: (i) the bulk supercooling prior to the nucleation of a phase, (ii) the cooling rates during solidification, (iii) the alloy composition, and (iv) the level of fluid flow during solidification.

It should be noted that the solidification path of a liquid phase separated into two liquid phases is considerably different and more complicated than that of a single supercooled liquid. This is mainly due to the fact that each liquid phase not only experiences a supercooling which can be considerably different from the bulk supercooling, but it can also follow a solidification path considerably different from that of the bulk composition.

5. SUMMARY

The microstructure of Cu-Fe-Co and Cu-Fe-Ni-Cr alloys under different solidification conditions was investigated, yielding the following results:

1) The first phase to solidify under slow cooling rates in Cu-Fe-Co and Fe-Cr-Ni-Cu alloys will be an γ-Fe phase. The composition of this phase is not constant. X-ray diffraction studies indicate that the structure parameters are of the γ-Fe phase and depend on the Co concentration in the dendrites. At a certain temperature a peritectic reaction will take place, in which some of the primary γ-Fe phase reacts with the remaining liquid to form an ε-Cu phase. As the peritectic reaction continues, the ε-Cu grows around the α-Fe dendrites until the latter are completely surrounded. Then the peritectic reaction slows down drastically due to the limited solid-state diffusion. The remaining liquid solidifies as an ε-Cu phase.

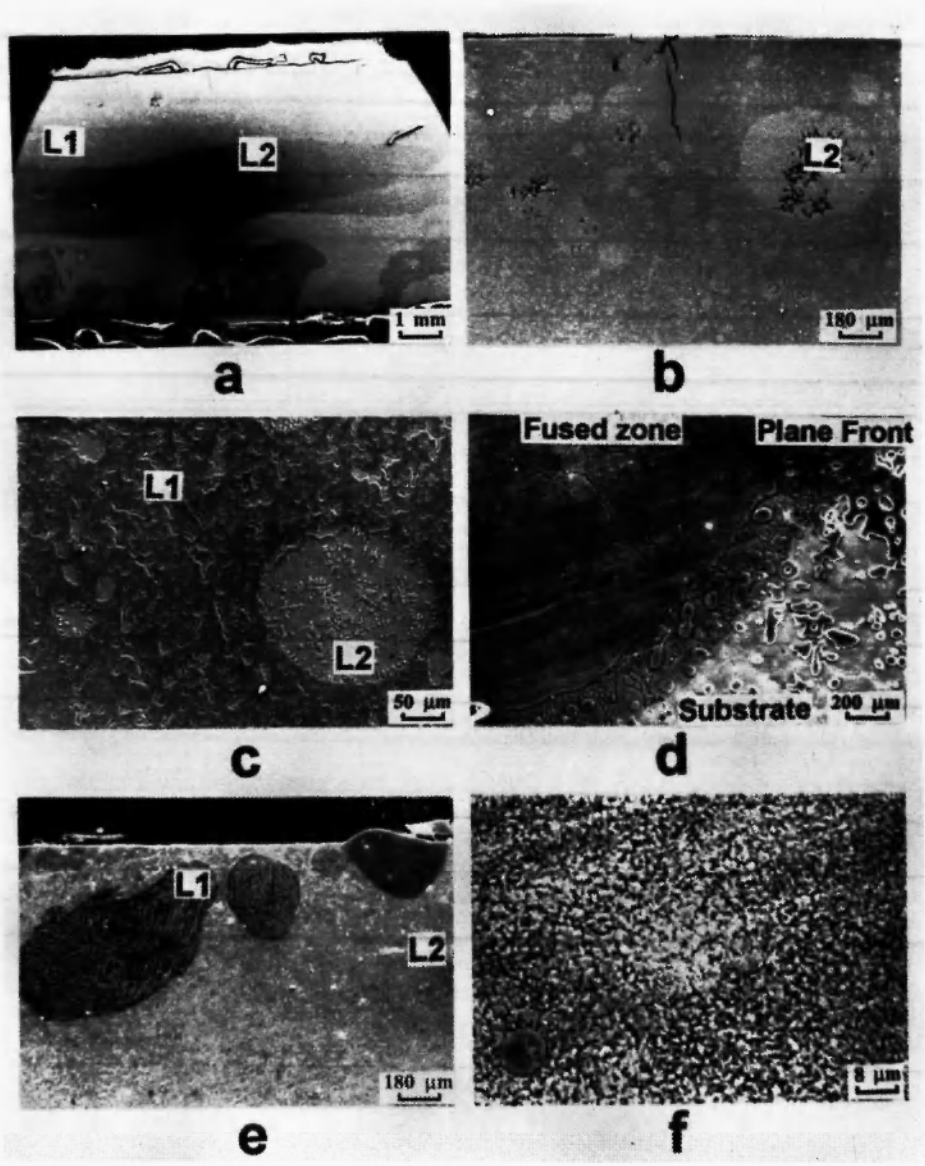

Fig. 4: Secondary electron images illustrating an electron beam melted surface of an arc melted Cu-47.3 wt.% Fe-5.1 wt.% Ni-14.1 wt.% Cr alloy. (a) an overall view demonstrating massive melt separation during the arc melt, (b)-(c) arc melt microstructure of primary L1 liquid in two magnifications, (d) higher magnification of the fused zone in the primary L1 liquid, (e) microstructure of primary L2 liquid, (f) microstructure of EB fused zone in the primary L2 liquid.

2) Bulk supercooling of Cu-Fe-Co and Cu-Fe-Ni-Cr alloys below the characteristic separation temperature, T_{SEP}, causes a metastable liquid separation into two liquids, one Cu-poor (L1) and the other Cu-rich (L2). Each of the liquids solidifies following a path dictated by the stable phase boundaries. The microstructure consisted of spherulites embedded in a matrix. The spherulites in alloys which contain more than 50 wt.% Cu solidify from the L1 melt, while in alloys which contain less than 50 wt.% Cu, they solidify from the L2 melt.
3) Secondary melt separation was observed in which each liquid further decomposed into two liquids.
4) Cu-Fe-Ni-Cr alloys containing less than 50 wt.%

Cu have a tendency to undergo complete melt separation. It might be that the C present in the melt causes this effect and not the other elements.

5) During the arc melting, Cu evaporation takes place which reduces the actual Cu concentration in the alloys.

ACKNOWLEDGEMENTS

The authors wish to thank Dr. Z. Burshtien for his critical reading of the manuscript.

REFERENCES

1. Z. Livne and a. Munitz, *J. Mater. Sci.*, **22**, 495 (1987).
2. A. Munitz, "Metastable liquid phase separation in TIG and electron beam copper/stainless-steel welds", *J. Mater. Sci.*, submitted.
3. A. Munitz, S. Elder and G.J. Abbaschian, *Met. Trans. A*, **23A**, 1817-1827 (1992).
4. H. Jones, in: *Treatise on Materials Science and Technology*, Vol. 20, H. Herman (ed.), Academic Press, New York, 1981; p. 1.
5. R. Mehrabian, *International Metals Reviews*, **27**, 185 (1982).
6. S.J.B. Reed, *Electron Microprobe Analysis*, Cambridge University Press, Cambridge, 1977; pp. 175-197.
7. A. Munitz, *Metall. Trans. B*, **11B**, 563 (1980).
8. A. Munitz and R. Abbaschian, "Supercooling and liquid separation in Cu-Co alloys solidified at different cooling rates", unpublished work.
9. S.P. Elder, A. Munitz and R. Abbaschian, *Materials Sci. Forum*, **50**, 137 (1989).
10. W.A. Tiller, K.A. Jackson, J.W. Rutter and B. Chalmers, *Acta Metall.*, **1**, 428 (1953).
11. T.W. Clyne, *Met. Trans. B*, **15B**, 369 (1983).